

This is an Open Access document downloaded from ORCA, Cardiff University's institutional repository: <https://orca.cardiff.ac.uk/id/eprint/129344/>

This is the author's version of a work that was submitted to / accepted for publication.

Citation for final published version:

Robinson, Andrew J., Hopkins, Goitseone L., Rastogi, Namrata, Hodges, Marie, Doyle, Michelle, Davies, Sara, Hole, Paul S., Omidvar, Nader, Darley, Richard L. and Tonks, Alex 2020. Reactive oxygen species drive proliferation in acute myeloid leukemia via the glycolytic regulator PFKFB3. *Cancer Research* 80 (5), pp. 937-949. 10.1158/0008-5472.CAN-19-1920

Publishers page: <http://dx.doi.org/10.1158/0008-5472.CAN-19-1920>

Please note:

Changes made as a result of publishing processes such as copy-editing, formatting and page numbers may not be reflected in this version. For the definitive version of this publication, please refer to the published source. You are advised to consult the publisher's version if you wish to cite this paper.

This version is being made available in accordance with publisher policies. See <http://orca.cf.ac.uk/policies.html> for usage policies. Copyright and moral rights for publications made available in ORCA are retained by the copyright holders.



1 **Article Title: Reactive oxygen species drive proliferation in acute myeloid leukemia via the**  
2 **glycolytic regulator PFKFB3**

3 **Running Title: ROS drives proliferation in AML via PFKFB3**

4 **Article Type: Original Article**

5 **Key Words:** Acute Myeloid Leukemia, Reactive Oxygen Species, Metabolism, Glycolysis,  
6 Proliferation.

7 **Authors/Affiliations:** Andrew J. Robinson,<sup>1</sup> Goitseone L. Hopkins,<sup>1</sup> Namrata Rastogi,<sup>1</sup> Marie  
8 Hodges,<sup>1,2</sup> Michelle Doyle,<sup>1,2</sup> Sara Davies,<sup>1</sup> Paul S. Hole,<sup>1</sup> Nader Omidvar,<sup>1</sup> Richard L. Darley<sup>1</sup>  
9 and Alex Tonks<sup>1‡,¥</sup>

10 <sup>1</sup>Department of Haematology, Division of Cancer & Genetics, School of Medicine, Cardiff  
11 University, Wales, United Kingdom.

12 <sup>2</sup>Cardiff Experimental and Cancer Medicine Centre (ECMC), School of Medicine, Cardiff  
13 University, Wales, United Kingdom.

14  
15 <sup>¥</sup>**Funding:**

16 This work was supported by grants from Tenovus Cancer Care (A.R), Bloodwise (13029),  
17 Medical Research Council (G.L.H.), Health and Care Research Wales (G.L.H; H07-3-06),  
18 Cancer Research UK (C7838/A25173) and Sêr Cymru II Fellow supported by Welsh  
19 Government, European Regional Development Fund (NR; 80762-CU-182)

20  
21 <sup>‡</sup>**Corresponding author:** Dr Alex Tonks, Department of Haematology, Division of Cancer &  
22 Genetics, School of Medicine, Cardiff University, Wales, UK.

23 Phone Number: ++44(0)2920742235

24 Email: Tonksa@cf.ac.uk

25 Twitter: @alex\_tonks

26 **Conflict of interest:** The authors declare no conflict of interest.

27 **Manuscript length:**

28 Abstract: 189

29 Manuscript length: 5313

30 References: 52

31 Figures: 7 figures

32 Supplemental files: 12 Supplemental Figures and 2 Supplemental Tables

33 **Abstract**

34 Acute myeloid leukemia (AML) is a heterogeneous clonal disorder with a poor clinical outcome.  
35 Previously we showed that overproduction of reactive oxygen species (ROS), arising from  
36 constitutive activation of NOX2 oxidase, occurs in >60% of AML patients and that ROS  
37 production promotes proliferation of AML cells. We show here that the process most  
38 significantly affected by ROS overproduction is glycolysis. Whole metabolome analysis of 20  
39 human primary AML showed that blasts generating high levels of ROS have increased glucose  
40 uptake and correspondingly increased glucose metabolism. In support of this, exogenous ROS  
41 increased glucose consumption whilst inhibition of NOX2 oxidase decreased glucose  
42 consumption. Mechanistically, ROS promoted uncoupling protein 2 (UCP2) protein expression  
43 and phosphorylation of AMPK, upregulating the expression of a key regulatory glycolytic  
44 enzyme, 6-phosphofructo-2-kinase/fructose-2,6-bisphosphatase (PFKFB3). Overexpression of  
45 PFKFB3 promoted glucose uptake and cell proliferation, whilst downregulation of PFKFB3  
46 strongly suppressed leukemia growth both in vitro and in vivo in the NSG model. These  
47 experiments provide direct evidence that oxidase-derived ROS promotes the growth of leukemia  
48 cells via the glycolytic regulator PFKFB3. Targeting PFKFB3 may therefore present a new mode  
49 of therapy for this disease with a poor outcome.

50 **Significance**

51 Findings show that ROS generated by NOX2 in AML cells promotes glycolysis by activating  
52 PFKFB3, and suggest PFKFB3 as a novel therapeutic target in AML.

53 **Introduction**

54 Reactive oxygen species (ROS) are a heterogeneous group of molecules and free radicals  
55 generated as a by-product of mitochondrial oxidative phosphorylation and deliberately generated  
56 via nicotinamide adenine dinucleotide phosphate (NADPH) oxidase (NOX) family proteins (1).  
57 In particular, NOX2 is expressed in the plasma membrane of hematopoietic cells that generates  
58 superoxide. Superoxide rapidly dismutates to hydrogen peroxide (H<sub>2</sub>O<sub>2</sub>), a relatively long-lived,  
59 mildly reactive molecule that traverses biological membranes and mediates redox signaling in  
60 both autocrine and paracrine fashion (2). The capacity of H<sub>2</sub>O<sub>2</sub> to reversibly oxidise cysteine  
61 residues in regulatory domains or active sites of proteins is believed to underlie its biological  
62 effects (3). Indeed, H<sub>2</sub>O<sub>2</sub> plays an integral role in hematopoiesis both through direct and indirect  
63 regulation of gene expression (4).

64 Excessive production of ROS is a common feature of cancer. In leukemia, ROS are known to  
65 cause DNA damage (5) and also promote proliferation (6-8). We previously showed that >60%  
66 of AML patients exhibited elevated levels of extracellular superoxide and H<sub>2</sub>O<sub>2</sub> which correlated  
67 with NOX2 expression (6). We also found that RAS (which is both directly and indirectly  
68 activated in AML (9)) was able to drive the production of NOX2-derived ROS in normal  
69 hematopoietic stem / progenitor cells (HSPC) and using this model we were able to show that  
70 RAS-induced ROS production contributed to the pro-proliferative effects of this oncogene (7).  
71 Despite this, the underlying mechanism through which ROS promote proliferation in cancer  
72 remains unclear. Using this model, we show for the first time that ROS particularly impacts on  
73 genes associated with the glycolytic pathway, with a key glycolytic regulator, PFKFB3, acting as  
74 an important mediator of ROS. Correspondingly, we show that ROS also promotes glycolysis in

75 cell lines and AML patient blasts. Furthermore, myeloid leukemia cells exhibit dependency on  
76 PFKFB3 both for their growth and survival. Given the frequently elevated levels of ROS in  
77 primary AML, these data provide a plausible mechanism for the enhanced glycolysis seen in  
78 AML and suggest that a therapeutic opportunity exists in which agents inhibiting PFKFB3 could  
79 be used to treat this disease.

## 80 **Materials and Methods**

### 81 **Key resources**

82 All reagents and key resources are provided in Supplemental material.

### 83 **Primary cell material and cell culture**

84 For whole cell metabolomics, a subset of bone marrow samples (n=20) from AML patients who  
85 had enrolled in UK MRC/NCRI AML clinical trials at point of diagnosis, before treatment and  
86 obtained informed written consent from patients in accordance with the 1964 Declaration of  
87 Helsinki, was used. Control mononuclear cells were isolated from peripheral blood of human  
88 male/female volunteers (n=6).

89 Human neonatal cord blood was obtained from healthy full-term pregnancies at the University  
90 Hospital Wales, Cardiff, UK. These were obtained with informed consent and with approval  
91 from the South East Wales Research Ethics Committee in accordance with the 1964 Declaration  
92 of Helsinki. Human CD34<sup>+</sup> cells (>95% pure, which constitute a mixed progenitor blood cell  
93 population) were isolated, cultured and transduced with retroviral vectors based on the PINCO  
94 backbone harboring either a GFP or DsRED selectable marker as previously described (10).  
95 Transduced human CD34<sup>+</sup> hematopoietic progenitor cells were cultured in supplemented IMDM

96 as previously described (10) containing 20% *v/v* FCS; supplemented with 5 ng/mL human (hu)  
97 IL-3, huG-CSF and huGM-CSF and 20 ng/mL huSCF. For microarray studies, on day 5 of  
98 culture (post CD34<sup>+</sup> isolation), cells were washed in PBS and resuspended in supplemented  
99 IMDM in the presence or absence of 100nM diphenyleiiodonium (DPI) for 18 h prior to  
100 Affymetrix microarray (n=4). RNA was extracted using Trizol<sup>®</sup> as previously described (11).  
101 Due to the high frequency of retroviral transduction (~70%), enrichment of transduced cells was  
102 unnecessary.

103 Cell lines were purchased from ATCC or ECACC and cultured according to recommended  
104 conditions at 37°C, 5% CO<sub>2</sub> for all experiments. All lines are maintained at ≤ 20 passage from  
105 receipt. The genetic identity of the cell lines was confirmed by short tandem repeat (STR) at  
106 purchase. Monthly monitoring for Mycoplasma contamination was performed and confirmed  
107 using the MycoAlert Detection Kit (Sigma). Mice were bred and maintained at Cardiff  
108 University (UK) and were cared for in accordance with Institutional Animal Care and Use  
109 Committee guidelines. NOD-SCID IL2R $\gamma^{(-/-)}$ (NSG) female mice were sub-lethally irradiated  
110 with 200cGy total body irradiation 24h before inoculation of THP-1 cells via tail-vein injection.  
111 Transplanted cells were analysed using hCD45-FITC, hCD33-APC and mCD45-PerCP-Cy5.5 by  
112 flow cytometry. For *ex vivo* analysis of mouse MRP8 N-RAS<sup>G12D</sup> leukemia (12), bone marrow  
113 was harvested from the tibias and glucose uptake was measured using 2-NBDG as described  
114 below.

### 115 **Detection of superoxide**

116 Following gene transduction, the indicated cell cultures were adjusted for viable cell number and  
117 superoxide measurement was carried out using the chemiluminescent probe Diogenes<sup>™</sup>

118 (Geneflow, U.K.). Briefly, cells were resuspended in their conditioned medium to a density of  
119  $1 \times 10^6$  cells/mL and 150  $\mu$ L aliquots were assayed in triplicate in FluoroNunc Maxisorp 96 well  
120 plates (Thermo-Fisher Scientific, Loughborough, UK). Diogenes (50  $\mu$ L) was added  
121 immediately prior to recording chemiluminescence as previously described (7).

122

### 123 **Determination of glucose and lactate**

124 Supernatant from the culture media was filtered using Microcon-10 kDa centrifugal filter units  
125 (Merck-Millipore, Feltham, UK) at  $12,782 \times g$  for 30 min. The levels of D-glucose and L-  
126 Lactate were measured by fluorimetry using a glucose and L-Lactate assay kit (Abcam,  
127 Cambridge, UK) coupled with a Chameleon Hidex fluorescent plate reader (Ex/Em 535/590 nm),  
128 according to the manufacturer's instructions. Briefly, samples were diluted with proprietary  
129 glucose or lactate buffer to a volume of 50 $\mu$ L and added in triplicate to a black 96 well flat  
130 bottomed microclear plate (Greiner Bio-One, Stonehouse, UK). Glucose or lactate buffer  
131 containing proprietary glucose or lactate probe (0.8% v/v) and proprietary glucose or lactate  
132 enzyme mix (0.8% v/v) were added (50 $\mu$ L) to each well and left to incubate in the dark at RT for  
133 30 min. Fluorescence was measured (Ex/Em 535/590nm) and compared with glucose or lactate  
134 standards assayed in duplicate on the same plate.

135 To determine cellular glucose uptake at the individual cell level, the glucose bioprobe 2-NBDG  
136 (Life Technologies, U.K.) was employed in conjunction with flow cytometry. Cells were  
137 washed twice in PBS then treated with 2-NBDG (10 $\mu$ M) or PBS alone (to establish a  
138 background control) followed by incubation for 10 min (37°C, 5% CO<sub>2</sub>) and two washes in ice  
139 cold PBS. Cells were immediately analysed by flow cytometry using an Acurri C6 flow  
140 cytometer. 2-NBDG emits fluorescence at a wavelength of 542nm. Having excluded cell debris

141 based on FSC/SSC, the median glucose uptake per cell of the samples was established by  
142 subtracting the median value of fluorescence of the background control cells from the median  
143 value of fluorescence of the cells treated with 2-NBDG. In some experiments, cells were treated  
144 with PEGylated catalase (300 mU/mL) for 24 h at 37°C, prior to analysis of glucose uptake.

#### 145 **Expression analysis**

146 Transduced CD34<sup>+</sup> cells were washed in PBS and resuspended in supplemented IMDM in the  
147 presence or absence of 100nM diphenyleneiodonium (DPI) for 18 h prior to RNA isolation (n=4)  
148 as previously described (11). RNA was hybridized to Affymetrix GeneChip<sup>®</sup> Human Exon 1.0<sup>ST</sup>  
149 Array for whole-transcript expression analysis. Data were analysed using Partek Genomics Suite  
150 (v6.6; Partek, MO, USA). Data analysis of CEL files are described in Supplemental Methods;  
151 data available at <https://www.ebi.ac.uk/arrayexpress> (accession number e-mexp-583). Gene  
152 Ontology (GO) enrichment analysis was undertaken using Metacore<sup>®</sup> (Clarivate Analytics,  
153 U.K.).

154 Detection of each protein was determined by western blot using antibodies described in  
155 Supplemental Methods, in conjunction Amersham ECL<sup>™</sup> Advance/Prime Western Blotting  
156 Detection Kit (GE Healthcare U.K.).

#### 157 **Metabolomics**

158 Metabolomic analysis of AML patient blast samples or Mv4;11 was carried out by Metabolon<sup>™</sup>  
159 (<http://www.metabolon.com/>). Data was generated using ultra-high performance liquid  
160 chromatography-tandem mass spectroscopy (UPLC-MS/MS) and gas-chromatography mass-  
161 spectroscopy (GC-MS). Peripheral blood and bone marrow samples collected from a random

162 cohort of AML patients were counted and analysed for viability using 7-AAD. Only those  
163 samples with a cell count greater than 30 million and a viability greater than 80% were sent for  
164 analysis by Metabolon™ (n=20). Additionally, mononuclear cells isolated from healthy  
165 individuals (n=6) were also sent to Metabolon™ as a comparative control. Diogenes™ analysis  
166 of AML blasts stratified the patient samples into ROS<sup>High</sup> (above median) and ROS<sup>Low</sup> (below  
167 median). Raw data was extracted, peak identified and quality control processed using  
168 proprietary Metabolon™ hardware, software and biochemical library database. Following  
169 normalisation to Bradford protein concentration, log transformation and imputation of missing  
170 values with the minimum observed value for each compound, Welch's unequal variance two  
171 sample t-test was performed to identify significant differences between the experimental groups.  
172 To account for a potentially high false discovery rate (as a consequence of multiple  
173 comparisons), a q-value was also calculated, where a lower q-value is an indication of higher  
174 confidence in the result.

#### 175 **Protein expression analysis of genes identified by microarray analysis**

176 Detection of each protein (see key resources table) was determined using a monoclonal or  
177 polyclonal antibody in conjunction with an anti-mouse or anti-Rabbit HRP linked secondary  
178 antibody and Amersham ECL™ Advance/Prime Western Blotting Detection Kit (GE Healthcare  
179 UK) according to the manufacturer's instruction. In the case of NOX2 or glucose transporter cell  
180 surface protein expression, PE conjugated antibody to NOX2 epitope or an indirect stain coupled  
181 with anti-mouse IgG-APC was used and protein expression was determined by flow cytometry.

#### 182 **Flow cytometric and data analysis**

183 Flow cytometric data were acquired using an Accuri C6 cytometer (BD, U.K.). Data analysis  
184 was performed using FCS express v6 (DeNovo Software). The threshold for GFP positivity was  
185 determined from the autofluorescence of GFP/DsRED negative cells in mock transduced  
186 cultures. Significance of difference was tested using Minitab software version 19 (Minitab Inc,  
187 PA) all analyses except those provided by Metabolon assays (see above). Appropriate statistical  
188 tests used are labelled in figure legends. To better understand variations between samples,  
189 principal component analysis (PCA) or hierarchical clustering using distance Pearson Correlation  
190 was employed to provide a global analysis of how closely related or otherwise any given sample  
191 is (mRNA or biochemical).

## 192 **Results**

### 193 **NOX-derived ROS promotes transcriptional change in N-RAS<sup>G12D</sup> expressing** 194 **hematopoietic progenitor cells and AML patient blasts**

195 We previously showed that expression of N-RAS<sup>G12D</sup> in HSPC strongly promotes ROS  
196 production through activation of NOX oxidases leading to increased proliferation (7). We used  
197 this model of ROS overproduction in primary hematopoietic CD34<sup>+</sup> cells (Supplemental Fig.  
198 S1A-E) to investigate the changes in gene expression mediated by ROS. We reasoned that we  
199 could enrich for ROS target genes by looking for gene changes which were absent in mutant N-  
200 RAS<sup>G12D</sup> cells treated with the NOX inhibitor, DPI (Fig. 1A). N-RAS<sup>G12D</sup> significantly changed  
201 the expression of 305 genes in HSPC (p<0.05) (Supplemental Table S1) of which 24 were  
202 specifically attributed to ROS production. Metacore<sup>TM</sup> pathway analysis identified glycolysis as  
203 the most dysregulated pathway (Fig. 1B). ROS significantly impacted the expression of 18% of  
204 genes involved in carbohydrate metabolism (Fig. 1C). To examine this in AML patient blasts,

205 we analyzed the TCGA database of 161 AML patients using cBioPortal (13, 14). Hierarchical  
206 clustering in Fig. 1D shows that patients with high NOX2 (*CYBB*) expression (which we have  
207 previously shown to correlate with ROS production (7)) clustered together based on correlative  
208 expression of genes involved in carbohydrate metabolism suggesting changes in glucose  
209 utilization compared to those patients with lower NOX2 expression; more than half the ROS  
210 regulated genes observed above are seen in this cluster. Fig. 1E shows the ROS-responsive  
211 genes that significantly correlated with NOX2 expression in AML blasts. Data derived from  
212 TCGA (15) supports the overexpression of *NOX2* mRNA in AML (Supplemental Fig. S2A).  
213 Increased *NOX2* expression also showed a trend towards poor prognosis (P=0.075; Supplemental  
214 Fig. S2B). We did not observe any significant association of expression of genes identified in  
215 Fig.1E with AML cytogenetics or survival. Taken together, these data show that NOX inhibition  
216 upregulates the expression of genes involved in carbohydrate metabolism.

### 217 **ROS promotes functional changes in glucose uptake**

218 Increased aerobic glycolysis is a common feature of cancerous cells with concomitant increases  
219 in cellular glucose uptake and lactate secretion (16). In order to assess whether transcriptional  
220 changes observed above resulted in functional glycolytic changes, glucose uptake and lactate  
221 secretion were measured. The level of glucose taken up by N-RAS<sup>G12D</sup> HSPC was significantly  
222 more (48±19%) when compared to control (Fig. 2A) when analysing glucose remaining in the  
223 culture media. To confirm that these changes in cellular glucose consumption occurred at the  
224 single cell level, the fluorescent glucose bioprobe 2-NBDG was employed (Supplemental Fig.  
225 S3). N-RAS<sup>G12D</sup> increased glucose uptake by 36±15% compared to controls (Fig. 2A). To  
226 support these *in vitro* data, glucose uptake was assayed *ex vivo* in bone marrow cells harvested  
227 from secondary transplants of transgenic mice expressing N-RAS<sup>G12D</sup> (12). A significant

228 90±48% increase in glucose uptake was observed in N-RAS<sup>G12D</sup> mice compared to wild type  
229 control (Fig. 2B). These data demonstrate that expression of mutant N-RAS<sup>G12D</sup> increases  
230 glucose uptake both *in vitro* and *ex vivo*.

231 To assess whether increases in glucose uptake were mediated by NOX-derived ROS, we  
232 examined the effect of the NOX inhibitor, DPI, on N-RAS<sup>G12D</sup> HSPC. NOX inhibition reduced  
233 glucose uptake by 20% compared to untreated cells (Fig. 2C) when analysing glucose remaining  
234 in the culture media. Similar data were obtained with the alternative NOX inhibitor, VAS-2870  
235 (17). Treatment with PEGylated catalase (which catabolises the destruction of H<sub>2</sub>O<sub>2</sub> at the  
236 plasma membrane (18)) also reverted the increase in glucose uptake (Fig. 2C). In contrast,  
237 treatment of control HSPC with DPI or VAS-2870 had no significant effect on glucose uptake.  
238 To determine whether these changes in glucose uptake resulted in increases in extracellular  
239 lactate production, levels of L-lactate in the culture supernatant were assayed. Interestingly, no  
240 significant changes in lactate secretion (see below) was observed in cells expressing N-RAS<sup>G12D</sup>  
241 compared to control (Fig. 2D).

## 242 **Overproduction of ROS is associated with changes in glucose utilization in primary AML** 243 **blasts**

244 The above data suggests increased glucose uptake is at least in part mediated by production of  
245 NOX-derived ROS. To establish evidence for this in primary AML, we stratified AML blasts  
246 according to extracellular ROS production (ROS<sup>High</sup> and ROS<sup>Low</sup>; Supplemental Fig. S4A-B) and  
247 analysed the global biochemical metabolomic profile. Using this approach, 444 named  
248 metabolites were identified which distinguished ROS<sup>High</sup>, ROS<sup>Low</sup> and control MNC by PCA  
249 (Fig. 3A). A summary of the biochemicals that achieved statistical significance ( $p \leq 0.05$ ) or

250 approached it ( $0.05 < p < 0.10$ ), is shown in Fig. 3B and in full in Supplemental Table S2. Random  
251 Forest (RF) analysis of the cellular metabolic profiles resulted in 85% predication accuracy in  
252 differentiating ROS<sup>High</sup> and ROS<sup>Low</sup> groups (Supplemental Fig. S5). Among the 30 top-ranking  
253 metabolites resulting from the RF analyses were biochemicals spanning different pathways, but  
254 primarily limited to those associated with nucleotides and lipid metabolism. Polyunsaturated  
255 fatty acids and lipid-related changes in n3 and n6 polyunsaturated fatty acids showed significant  
256 accumulations within the AML<sup>High</sup> compared to the AML<sup>Low</sup> samples which would be indicative  
257 of increased uptake (Supplemental Table S2). Interesting, within the AML<sup>High</sup> samples,  
258 lysolipids, monoacylglycerols and glycerol were consistently and significantly higher in relation  
259 to AML<sup>Low</sup> ROS (see discussion).

260 Focussing specifically on detected metabolites within the glycolytic pathway, we found, glucose,  
261 glucose-6-phosphate and fructose-6-phosphate levels were significantly higher within the  
262 ROS<sup>High</sup> blasts compared to ROS<sup>Low</sup> blasts indicating that increased glucose utilisation correlates  
263 with elevated ROS (Fig. 3C). In agreement with our *in vitro* HSPC model, changes in lactate  
264 were not significantly different between the ROS high and ROS low groups but were higher than  
265 the control MNC (Fig. 3C). This suggests that whilst glucose utilisation is increased in primary  
266 AML, higher levels of ROS are consistent with increased levels of glycolytic intermediates.  
267 Indeed, metabolites associated with the pentose phosphate pathway (PPP) including the isobaric  
268 compound ribulose/xylulose 5-phosphate and sedoheptulose-7-phosphate were also higher in  
269 ROS<sup>High</sup> vs ROS<sup>Low</sup> samples (Fig. 3D). We next set out to determine whether the addition of  
270 exogenous H<sub>2</sub>O<sub>2</sub> to the ROS<sup>Low</sup> AML cell line, Mv4;11 could itself promote changes in glucose  
271 metabolism. Similarly to primary AML-ROS<sup>high</sup> we observed an increase in glucose  
272 consumption (Fig. 4) and biochemicals associated with the PPP (Supplemental Fig. S6A and B).

273 Taken together these data suggests increased glucose utilization by PPP, potentially driving  
274 nucleotide biosynthesis and NAD(P)H generation within ROS<sup>High</sup> blasts.

### 275 **PFKFB3 is a ROS responsive target that mediates changes in glucose utilization**

276 The data above suggest that ROS-induced changes in mRNA expression of genes of glycolysis  
277 (Fig. 1C) was associated with altered glucose utilization (Fig. 3). To validate these findings, we  
278 surveyed the expression of these ROS-responsive genes at the protein level (Supplemental Fig.  
279 S7A-D). ROS induced changes at the protein level, only occurred in the expression of the  
280 regulatory glycolytic enzyme 6-phosphofructo-2-kinase/fructose-2,6-bisphosphatase 3  
281 (PFKFB3)(Fig. 4A and Supplemental Fig. S7A). PFKFB is a bifunctional enzyme with both  
282 kinase and phosphatase activity that regulates the glycolytic pathway (19). To support this data,  
283 we inhibited NOX derived ROS production in the ROS<sup>High</sup> AML cell line, THP-1, using NOX2  
284 knock-down (Supplemental Fig. S8A-C). In line with our previous data (7), NOX inhibition  
285 with DPI suppressed proliferation of N-RAS<sup>G12D</sup> cells. As shown in Fig. 4B, loss of NOX2  
286 protein expression and ablation of superoxide production in these cells reduced the expression of  
287 PFKFB3 compared to control cells with a concomitant reduction in proliferation by 30±12%  
288 when compared to control (Fig. 4C). Glucose uptake was similarly reduced by 25±17% (Fig.  
289 4D). We next set out to determine whether the addition of exogenous H<sub>2</sub>O<sub>2</sub> to the ROS<sup>Low</sup> AML  
290 cell line, Mv4;11 cells, could itself promote PFKFB3 protein expression. As predicted, we  
291 observed a dose-dependent increase in PFKFB3 protein expression (Fig. 4E) with concomitant  
292 increases in proliferation (Fig. 4F and Supplemental Fig. S9) and glucose uptake (Fig. 4G).

293 To investigate whether PFKFB3 itself could mediate these phenotypic changes, we  
294 overexpressed PFKFB3 in Mv4;11 cells (PFKFB3-OE; Fig. 5A). Cells overexpressing PFKFB3

295 showed a  $72\pm 30\%$  increase in proliferation (at 72 h) compared to control cells (Fig. 5B) and  
296 correspondingly showed an increased proportion of cells in S+G2M phase of the cell cycle  
297 (Supplemental Fig. S10A). The levels of glucose uptake in PFKFB3-OE cells were significantly  
298 more ( $35\pm 2\%$ ) compared to control cells (Fig. 5C). To determine the impact of decreased  
299 expression of PFKFB3 in ROS generating cells, PFKFB3 was knocked-down in THP-1 cells  
300 (Fig. 5D). Knock-down of PFKFB3 resulted in reduced proliferation of these cells (Fig. 5E) and  
301 a reduction in the percentage of cells in cycle (Supplemental Fig S10B), though without  
302 detectable change in glucose uptake in this context (Fig. 5F). These experiments provide the  
303 first direct evidence that PFKFB3 controls the growth of leukemia cells which is consistent with  
304 cells producing high levels of ROS.

### 305 **ROS induced changes in PFKFB3 expression are mediated via UCP/p-AMPK**

306 To determine the mechanism of ROS induced PFKFB3 expression we analysed two potential  
307 mechanisms. Firstly, HIF-1 $\alpha$  has been shown to induce increased *PFKFB3* mRNA expression  
308 (20). Analysing our transcriptome data revealed that *HIF-1 $\alpha$*  is a strongly ROS-responsive gene  
309 (Fig. 6A). However, we were unable to detect expression of HIF1- $\alpha$  protein regardless of NOX2  
310 status (Fig. 6B). Furthermore, HIF1 $\alpha$  knock-down (Fig. 6B) did not change PFKFB3 protein  
311 expression (Fig. 6C) or glucose uptake (Fig. 6D). Collectively, these data do not therefore  
312 support a role of HIF1- $\alpha$  in mediating glycolytic changes in these cells.

313 Superoxide levels are sensed by uncoupling protein 2 (UCP2) which drives an adaptive response  
314 to protect against oxidative stress including the activation of AMP-activated protein kinase  
315 (AMPK) (21) leading to increased production of PFKFB3 (22). In accord with this we observed

316 that treatment of the ROS<sup>Low</sup> AML cell line, Mv4;11, with exogenous H<sub>2</sub>O<sub>2</sub> increased both  
317 PFKFB3 expression and AMPK phosphorylation (Fig. 6E). This induction was inhibited by  
318 Genipin (which specifically inhibits UCP2 expression (23)) decreasing both p-AMPK and  
319 PFKFB3 levels (Fig. 6D) and concomitant reduction in glucose consumption (Fig. 6F). To  
320 confirm, changes in p-AMPK/mTOR signalling, we next examined downstream signalling of  
321 mTOR by western blot. As shown in Supplemental Fig. S11A and B phosphorylation of S6  
322 kinase is decreased following treatment with H<sub>2</sub>O<sub>2</sub>; an effect reversed when UCP2 is inhibited.  
323 These data support a role for UCP2 having a pivotal role in mediating ROS-induced changes in  
324 the expression of PFKFB3.

### 325 **Targeting PFKFB3 reduces glucose uptake and cell proliferation in AML cells**

326 We next wanted to establish whether chemical inhibition of PFKFB3 could have the potential for  
327 a therapeutic impact in the treatment of AML. Having established appropriate inhibitory  
328 concentrations of two chemical inhibitors of PFKFB3, 3-(3-pyridinyl)-1-(4-pyridinyl)-2-propen-  
329 1-one (3PO) (24) and the more specific PFK158 (25) (Supplemental Fig. S12A-C). We next  
330 treated ROS<sup>High</sup> cells (THP-1) with 3-PO or PFK158 which resulted in a reduction in glucose  
331 uptake (Fig. 7A and B). Correspondingly, treatment with 3PO resulted in a significant dose  
332 dependent decrease in proliferation of THP-1 cells (Fig. 7C) whilst treatment with the more  
333 specific PFK158 (25) also significantly reduced proliferation at doses >500nM (Fig. 7D). We  
334 next investigated whether PFKFB3 inhibition could suppress the effects of exogenous ROS on  
335 the ROS<sup>Low</sup> cell line Mv4;11. No change in viability in Mv4;11 (or THP-1) cells treated with  
336 3PO, PFK158 or H<sub>2</sub>O<sub>2</sub> were observed. Treatment of Mv4;11 cells with H<sub>2</sub>O<sub>2</sub> resulted in a  
337 20±9% increase in glucose uptake compared with control (as expected), whilst combined  
338 treatment with H<sub>2</sub>O<sub>2</sub> and 3PO or with PFK158 inhibitor ablated the response to peroxide (Fig.

339 7E). Treatment with these inhibitors alone did not alter glucose uptake when compared to  
340 control cells.

341 Finally, we investigated whether loss of PFKFB3 also affected leukemia growth *in vivo*. Knock-  
342 down of PFKFB3 expression in THP-1 cells resulted in a significant reduction (83%) of  
343 leukemia cell growth, supporting a role of PFKFB3 in the proliferation of AML cells *in vivo*  
344 (Fig. 7F). Overall these experiments provide the first direct evidence that oxidase-derived ROS  
345 promotes the growth of leukemia cells via PFKFB3 expression and suggests a potential ROS-  
346 dependent mechanism for these changes.

## 347 **Discussion**

348 Whilst increased levels of ROS produced by AML blasts or tumor cells have been shown to  
349 induce double strand breaks (26), they also promote proliferation (6, 27). Here we present  
350 evidence that the proliferative response to ROS is supported by changes in glucose uptake and  
351 altered glucose metabolism. Furthermore, we demonstrate that AML cells exhibit enhanced  
352 PFKFB3 expression and that inhibitors that target the function of this protein (or its upstream  
353 pathway UCP2/AMPK) may provide a tractable therapeutic target in AML.

354 ROS are now recognized as important secondary messengers, serving as critical cell signaling  
355 molecules through the capacity of H<sub>2</sub>O<sub>2</sub> to reversibly oxidise cysteine residues (28). Using a  
356 primary cell model for ROS production, we investigated the effect of ROS on gene transcription  
357 and found that changes in mRNA expression were associated with enzymes involved in glucose  
358 metabolism. Specifically, we identified several gene changes associated with glycolysis coupled  
359 with increased cellular glucose uptake. This is consistent with many solid tumor models that

360 shift energy production from oxidative phosphorylation toward the less efficient glycolytic  
361 pathway, a phenomenon known as the Warburg effect (29). Indeed, our previous data have  
362 shown no significant differences in mitochondrial ROS were observed in mutant Ras expressing  
363 CD34<sup>+</sup> cells compared to controls (7). Using inhibitors to NOX2, we were able to attribute the  
364 effects of observed increases in glucose uptake to the production of extracellular NOX2-derived  
365 ROS. Additionally, we found leukemic cell lines increased glucose uptake in response to  
366 exogenous ROS or showed decreased uptake following NOX2 knock-down. We show for the  
367 first time that the effect of ROS on glucose uptake is mediated by PFKFB3 (see below).  
368 However, pro-glycolytic effects of ROS on other genes have been observed (30) and is  
369 consistent with increased glycolysis in solid tumor models associated with GLUT upregulation  
370 (31).

371 In the context of primary AML, we previously demonstrated that >60% of patients exhibited  
372 high levels of ROS which correlated with NOX2 expression (6). Here, AML blasts stratified  
373 according to level of extracellular ROS production were analysed by global biochemical  
374 metabolomic profiling. Several hundred metabolites were identified which distinguished  
375 patients according to ROS production including metabolite levels within the glycolytic pathway  
376 (glucose, glucose-6-phosphate and fructose-6-phosphate) suggesting that the impact of ROS is to  
377 increase the levels of glycolytic intermediates, primarily those in the early part of the glycolytic  
378 pathway. In support of this, metabolites associated with the PPP such as sedoheptulose-7-  
379 phosphate and the isobaric compounds ribulose/xylulose 5-phosphate were also elevated in  
380 ROS<sup>High</sup> samples. These data may be indicative of a reprogramming of metabolic pathways,  
381 where increased glucose consumption, is metabolised via the PPP, resulting in increased  
382 generation of NADPH (to counter oxidative stress) and biosynthetic precursors such as

383 nucleotides, necessary for cell growth and DNA repair. Interestingly, metabolomic profiling of  
384 serum from AML patients has also revealed distinct increases in the glycolytic metabolic (32,  
385 33). Additionally, NOX2 expression has previously been demonstrated to regulate self-renewal  
386 of leukemic stem cells (34). Using a murine model of leukemia, Adane *et al* showed that  
387 suppression of NOX2 expression led to increased fatty acid oxidation and potential limiting of  
388 substrates passing through glycolysis. Our study supports this notion, where we also observed  
389 significant changes associated with lipid metabolism in human AML; lipid-related changes in n3  
390 and n6 polyunsaturated fatty acids showed significant accumulations within the AML<sup>High</sup> in  
391 relation to the AML<sup>Low</sup> samples. The higher levels of monoacylglycerols and glycerol in the  
392 AML<sup>High</sup> samples may also be an indicator of increased lipolysis to support free fatty acid levels.  
393 Taken together, these data show that NOX2 derived ROS impact on glucose metabolism, an  
394 effect consistent with that seen in solid tumors (35).

395 We identified significant ROS induced changes in mRNA and in protein of the regulatory  
396 glycolytic enzyme PFKFB3. *PFKFB3* mRNA expression has been shown to be upregulated in  
397 several solid tumors including colon, breast, prostate, ovary, thyroid and head and neck  
398 squamous cell carcinoma (36, 37). Whilst *PFKFB3* mRNA is elevated in AML we did not  
399 observe any significant association of expression with particular AML subgroups or clinical  
400 outcome. PFKFB is a bifunctional enzyme, which catalyses both forward and reverse reaction of  
401 F-6-P to F-2,6-BP (19). In turn, F-2,6-BP is a powerful allosteric activator of PFK which  
402 catalyses F-6-P to F-1,6-BP, a rate limiting step in glycolysis. The PFKFB3 isoform contains a  
403 lysine and serine at position 79 and 80 respectively (38) resulting in increased kinase activity,  
404 which is 740 times greater than other PFKFB isoforms, making it a powerful driver of glycolysis  
405 (39). Here we also showed ROS dependent changes in PFKFB3 expression in AML lines with

406 constitutive NOX2 activity/ROS production coupled with suppression of reduction in  
407 proliferation and glucose uptake upon ROS inhibition. Overexpression/knock-down of PFKFB3  
408 generated the predicted changes in glucose uptake and cell proliferation *in vitro* whilst knock-  
409 down of PFKFB3 strongly suppresses leukemia growth *in vivo* (though we have not confirmed  
410 what the mechanistic basis of the effects are, *in vivo* data).

411 It has previously been established that ROS can regulate HIF-1 $\alpha$  in a non-hypoxic pathway (40).  
412 Further, stabilisation of HIF-1 $\alpha$  has been associated with increased expression of glycolytic  
413 genes, including PFKFB3 (41, 42). Our data showed increased expression of *HIF-1 $\alpha$*  mRNA  
414 correlated with increased ROS levels. However, immunoblotting showed that HIF-1 $\alpha$  was not  
415 expressed at detectable levels and furthermore knock-down of the mRNA for this protein did not  
416 result in any changes in glucose uptake. ROS has also previously been shown to activate  
417 mitochondrial proteins (UCP2) to regulate the leak of protons across the inner membrane,  
418 resulting in poor fuel conversion efficiency and a more pro-glycolytic phenotype including  
419 AMPK activation (21). We show that inhibition of UCP2 led to decreased p-AMPK and  
420 PFKFB3 levels. Further, analysis of the mTOR pathway showed decreased S6-Kinase  
421 expression in response to ROS which was reverted upon UCP inhibition. AMPK is a master  
422 regulator of cellular energy homeostasis, upregulating catabolic metabolic processes including  
423 increased glycolytic flux and protects against ROS accumulation by increasing NADPH  
424 production (see below) (17). AMPK has previously been shown to be activated via ROS (43), in  
425 addition to regulating glycolysis and PFKFB3 expression in a phosphorylation dependent  
426 manner in cancer cells (22, 44). Domenech *et al.*, have shown that mitotic arrest of cancer cells  
427 leads to altered energy requirements through switching to a more glycolytic phenotype and  
428 increased AMPK phosphorylation (22). This suggests that PFKFB3 could also be increased

429 through changes to cell cycle or autophagy. Metabolomic data generated as part of this study  
430 also indicated increased levels of ROS correlated with an increase in fatty acid metabolites  
431 (Supplemental Table S2). Interestingly, changes in expression of UCP2 has been linked with 2-3  
432 fold elevation of plasma fatty acids reviewed in (45). Further, activation of fatty acid  
433 metabolism by AMPK (46) is interesting given that ROS activation of AMPK has also been  
434 shown to potentially influence and maintain HSC (47). Conversely, inhibition of mitochondrial  
435 fatty acid oxidation induces loss of HSC maintenance (48).

436 Identification of metabolic differences between normal and malignant tissue creates a therapeutic  
437 opportunity for targeting of glycolysis in the treatment of AML; the potential for targeted therapy  
438 in AML, through reduction of aberrant metabolic activity via inhibition of 6-phosphogluconate  
439 dehydrogenase (6-PGD) function has also recently been shown (32). The therapeutic potential of  
440 PFKFB3 inhibition (e.g. PFK158) (25) in cancer is currently undergoing phase I clinical trials  
441 (49). Consistent with studies in solid tumors (50, 51), data presented here shows that in ROS<sup>High</sup>  
442 AML cells, treatment with PFKFB3 inhibitor significantly reduced glucose uptake and also  
443 proliferation both *in vitro* and *in vivo*. This supports a previous study which showed chemical  
444 inhibition of PFKFB3 in Jurkat T-cell leukemia cells results in decreased proliferation and  
445 glucose uptake (24). In myeloproliferative neoplasms expressing JAK2 mutations, PFKFB3 is  
446 required for increased growth and metabolic activity, an effect blocked by targeted knock-down  
447 of PFKFB3. This study therefore suggested that therapies specifically blocking PFKFB3  
448 activity/expression would be expected to inhibit JAK2/STAT5-dependent malignancies (52).

449 In conclusion, this and previous data suggest that production of ROS may confer a competitive  
450 advantage on premalignant/malignant cells by promoting the proliferation of these cells via

451 changes to carbohydrate metabolism. We show for the first time a link between increased NOX-  
452 derived ROS production and increased expression of the key glycolytic regulatory enzyme,  
453 PFKFB3. Furthermore, PFKFB3 inhibitors or genetic knock-down established a causal link  
454 between ROS production, cellular glucose uptake and PFKFB3 activity.

## 455 **Acknowledgments**

456 We are grateful to Nick Jones (Swansea University, Wales, UK) for critically appraising the  
457 manuscript. We would also like to thank Megan Musson CBS, Cardiff University for her  
458 technical expertise for Affymetrix Microarray. We are grateful to Prof Tee (Cardiff University)  
459 for his expertise in AMPK/mTOR signalling advice. The authors are grateful for support from  
460 the NCRI AML trials cell bank and the AML patients for providing primary samples used in this  
461 study. This work was supported by grants from Tenovus Cancer Care (A.R), Bloodwise  
462 (13029), Medical Research Council (G.L.H.) and Health and Care Research Wales (G.L.H; H07-  
463 3-06). NR is a Sêr Cymru II Fellow supported by Welsh Government, European Regional  
464 Development Fund (NR; 80762-CU-182).

## 465 **Supplemental Information**

466 Supplemental information is available at Cancer Research website.

## 467 **References**

468

469

470 (1) Lambeth JD, Neish AS. Nox enzymes and new thinking on reactive oxygen: a double-  
471 edged sword revisited. *Annu Rev Pathol* 2014;**9**:119-45.

- 472 (2) Hole PS, Darley RL, Tonks A. Do reactive oxygen species play a role in myeloid  
473 leukemias? *Blood* 2011;**117**:5816-26.
- 474 (3) Bindoli A, Rigobello MP. Principles in redox signaling: from chemistry to functional  
475 significance. *Antioxid Redox Signal* 2013;**18**:1557-93.
- 476 (4) Prieto-Bermejo R, Romo-Gonzalez M, Perez-Fernandez A, Ijurko C, Hernandez-  
477 Hernandez A. Reactive oxygen species in haematopoiesis: leukaemic cells take a walk on  
478 the wild side. *J Exp Clin Cancer Res* 2018;**37**:125.
- 479 (5) Mesbahi Y, Zekri A, Ghaffari SH, Tabatabaie PS, Ahmadian S, Ghavamzadeh A.  
480 Blockade of JAK2/STAT3 intensifies the anti-tumor activity of arsenic trioxide in acute  
481 myeloid leukemia cells: Novel synergistic mechanism via the mediation of reactive  
482 oxygen species. *Eur J Pharmacol* 2018;**834**:65-76.
- 483 (6) Hole PS, Zabkiewicz J, Munje C, Newton Z, Pearn L, White P, et al. Overproduction of  
484 NOX-derived ROS in AML promotes proliferation and is associated with defective  
485 oxidative stress signaling. *Blood* 2013;**122**:3322-30.
- 486 (7) Hole PS, Pearn L, Tonks AJ, James PE, Burnett AK, Darley RL, et al. Ras-induced  
487 reactive oxygen species promote growth factor-independent proliferation in human  
488 CD34+ hematopoietic progenitor cells. *Blood* 2010;**115**:1238-46.
- 489 (8) Jayavelu AK, Moloney JN, Bohmer FD, Cotter TG. NOX-driven ROS formation in cell  
490 transformation of FLT3-ITD-positive AML. *Exp Hematol* 2016;**44**:1113-22.
- 491 (9) Qian X, Nie X, Yao W, Klinghammer K, Sudhoff H, Kaufmann AM, et al. Reactive  
492 oxygen species in cancer stem cells of head and neck squamous cancer. *Semin Cancer  
493 Biol* 2018;**53**:248-57.
- 494 (10) Tonks A, Pearn L, Tonks AJ, Pearce L, Hoy T, Phillips S, et al. The AML1-ETO fusion  
495 gene promotes extensive self-renewal of human primary erythroid cells. *Blood*  
496 2003;**101**:624-32.
- 497 (11) Tonks A, Pearn L, Musson M, Gilkes A, Mills KI, Burnett AK, et al. Transcriptional  
498 dysregulation mediated by RUNX1-RUNX1T1 in normal human progenitor cells and in  
499 acute myeloid leukaemia. *Leukemia* 2007;**21**:2495-505.
- 500 (12) Omidvar N, Kogan S, Beurlet S, le PC, Janin A, West R, et al. BCL-2 and mutant NRAS  
501 interact physically and functionally in a mouse model of progressive myelodysplasia.  
502 *Cancer Res* 2007;**67**:11657-67.
- 503 (13) Gao J, Aksoy BA, Dogrusoz U, Dresdner G, Gross B, Sumer SO, et al. Integrative  
504 analysis of complex cancer genomics and clinical profiles using the cBioPortal. *Sci  
505 Signal* 2013;**6**:11.

- 506 (14) Cerami E, Gao J, Dogrusoz U, Gross BE, Sumer SO, Aksoy BA, et al. The cBio cancer  
507 genomics portal: an open platform for exploring multidimensional cancer genomics data.  
508 *Cancer Discov* 2012;**2**:401-4.
- 509 (15) Ley TJ, Miller C, Ding L, Raphael BJ, Mungall AJ, Robertson A, et al. Genomic and  
510 epigenomic landscapes of adult de novo acute myeloid leukemia. *N Engl J Med*  
511 2013;**368**:2059-74.
- 512 (16) Mikawa T, LLeonart ME, Takaori-Kondo A, Inagaki N, Yokode M, Kondoh H.  
513 Dysregulated glycolysis as an oncogenic event. *Cell Mol Life Sci* 2015;**72**:1881-92.
- 514 (17) Altenhofer S, Kleikers PW, Radermacher KA, Scheurer P, Rob Hermans JJ, Schiffers P,  
515 et al. The NOX toolbox: validating the role of NADPH oxidases in physiology and  
516 disease. *Cell Mol Life Sci* 2012;**69**:2327-43.
- 517 (18) Beckman JS, Minor RL, Jr., White CW, Repine JE, Rosen GM, Freeman BA. Superoxide  
518 dismutase and catalase conjugated to polyethylene glycol increases endothelial enzyme  
519 activity and oxidant resistance. *J Biol Chem* 1988;**263**:6884-92.
- 520 (19) Ros S, Schulze A. Balancing glycolytic flux: the role of 6-phosphofructo-2-  
521 kinase/fructose 2,6-bisphosphatases in cancer metabolism. *Cancer Metab* 2013;**1**:8.
- 522 (20) Yalcin A, Clem BF, Simmons A, Lane A, Nelson K, Clem AL, et al. Nuclear targeting of  
523 6-phosphofructo-2-kinase (PFKFB3) increases proliferation via cyclin-dependent  
524 kinases. *J Biol Chem* 2009;**284**:24223-32.
- 525 (21) Echtay KS, Roussel D, St-Pierre J, Jekabsons MB, Cadenas S, Stuart JA, et al.  
526 Superoxide activates mitochondrial uncoupling proteins. *Nature* 2002;**415**:96-9.
- 527 (22) Domenech E, Maestre C, Esteban-Martinez L, Partida D, Pascual R, Fernandez-Miranda  
528 G, et al. AMPK and PFKFB3 mediate glycolysis and survival in response to mitophagy  
529 during mitotic arrest. *Nat Cell Biol* 2015;**17**:1304-16.
- 530 (23) Mailloux RJ, Adjeitey CN, Harper ME. Genipin-induced inhibition of uncoupling  
531 protein-2 sensitizes drug-resistant cancer cells to cytotoxic agents. *PLoS One*  
532 2010;**5**:e13289.
- 533 (24) Clem B, Telang S, Clem A, Yalcin A, Meier J, Simmons A, et al. Small-molecule  
534 inhibition of 6-phosphofructo-2-kinase activity suppresses glycolytic flux and tumor  
535 growth. *Mol Cancer Ther* 2008;**7**:110-20.
- 536 (25) Clem BF, O'Neal J, Tapolsky G, Clem AL, Imbert-Fernandez Y, Kerr DA, et al.  
537 Targeting 6-phosphofructo-2-kinase (PFKFB3) as a therapeutic strategy against cancer.  
538 *Mol Cancer Ther* 2013;**12**:1461-70.
- 539 (26) Stanicka J, Russell EG, Woolley JF, Cotter TG. NADPH oxidase-generated hydrogen  
540 peroxide induces DNA damage in mutant FLT3-expressing leukemia cells. *J Biol Chem*  
541 2015;**290**:9348-61.

- 542 (27) Tang CT, Lin XL, Wu S, Liang Q, Yang L, Gao YJ, et al. NOX4-driven ROS formation  
543 regulates proliferation and apoptosis of gastric cancer cells through the GLI1 pathway.  
544 *Cell Signal* 2018;**46**:52-63.
- 545 (28) Paik JY, Jung KH, Lee JH, Park JW, Lee KH. Reactive oxygen species-driven HIF1alpha  
546 triggers accelerated glycolysis in endothelial cells exposed to low oxygen tension. *Nucl*  
547 *Med Biol* 2017;**45**:8-14.
- 548 (29) Koppenol WH, Bounds PL, Dang CV. Otto Warburg's contributions to current concepts  
549 of cancer metabolism. *Nat Rev Cancer* 2011;**11**:325-37.
- 550 (30) Prata C, Maraldi T, Fiorentini D, Zambonin L, Hakim G, Landi L. Nox-generated ROS  
551 modulate glucose uptake in a leukaemic cell line. *Free Radic Res* 2008;**42**:405-14.
- 552 (31) Macheda ML, Rogers S, Best JD. Molecular and cellular regulation of glucose  
553 transporter (GLUT) proteins in cancer. *J Cell Physiol* 2005;**202**:654-62.
- 554 (32) Chen WL, Wang JH, Zhao AH, Xu X, Wang YH, Chen TL, et al. A distinct glucose  
555 metabolism signature of acute myeloid leukemia with prognostic value. *Blood*  
556 2014;**124**:1645-54.
- 557 (33) Wang Y, Zhang L, Chen WL, Wang JH, Li N, Li JM, et al. Rapid diagnosis and  
558 prognosis of de novo acute myeloid leukemia by serum metabonomic analysis. *J*  
559 *Proteome Res* 2013;**12**:4393-401.
- 560 (34) Adane B, Ye H, Khan N, Pei S, Minhajuddin M, Stevens BM, et al. The Hematopoietic  
561 Oxidase NOX2 Regulates Self-Renewal of Leukemic Stem Cells. *Cell Rep* 2019;**27**:238-  
562 54.
- 563 (35) Shanmugam M, McBrayer SK, Rosen ST. Targeting the Warburg effect in hematological  
564 malignancies: from PET to therapy. *Curr Opin Oncol* 2009;**21**:531-6.
- 565 (36) Atsumi T, Chesney J, Metz C, Leng L, Donnelly S, Makita Z, et al. High expression of  
566 inducible 6-phosphofructo-2-kinase/fructose-2,6-bisphosphatase (iPFK-2; PFKFB3) in  
567 human cancers. *Cancer Res* 2002;**62**:5881-7.
- 568 (37) Li HM, Yang JG, Liu ZJ, Wang WM, Yu ZL, Ren JG, et al. Blockage of glycolysis by  
569 targeting PFKFB3 suppresses tumor growth and metastasis in head and neck squamous  
570 cell carcinoma. *J Exp Clin Cancer Res* 2017;**36**:7.
- 571 (38) Kim SG, Manes NP, El-Maghrabi MR, Lee YH. Crystal structure of the hypoxia-  
572 inducible form of 6-phosphofructo-2-kinase/fructose-2,6-bisphosphatase (PFKFB3): a  
573 possible new target for cancer therapy. *J Biol Chem* 2006;**281**:2939-44.
- 574 (39) Marsin AS, Bouzin C, Bertrand L, Hue L. The stimulation of glycolysis by hypoxia in  
575 activated monocytes is mediated by AMP-activated protein kinase and inducible 6-  
576 phosphofructo-2-kinase. *J Biol Chem* 2002;**277**:30778-83.

- 577 (40) Haddad JJ, Land SC. A non-hypoxic, ROS-sensitive pathway mediates TNF-alpha-  
578 dependent regulation of HIF-1alpha. *FEBS Lett* 2001;**505**:269-74.
- 579 (41) Chesney J, Telang S. Regulation of glycolytic and mitochondrial metabolism by ras. *Curr*  
580 *Pharm Biotechnol* 2013;**14**:251-60.
- 581 (42) Yalcin A, Telang S, Clem B, Chesney J. Regulation of glucose metabolism by 6-  
582 phosphofructo-2-kinase/fructose-2,6-bisphosphatases in cancer. *Exp Mol Pathol*  
583 2009;**86**:174-9.
- 584 (43) Shi SY, Lu SY, Sivasubramaniyam T, Revelo XS, Cai EP, Luk CT, et al. DJ-1 links  
585 muscle ROS production with metabolic reprogramming and systemic energy homeostasis  
586 in mice. *Nat Commun* 2015;**6**:7415.
- 587 (44) Novellademunt L, Bultot L, Manzano A, Ventura F, Rosa JL, Vertommen D, et al.  
588 PFKFB3 activation in cancer cells by the p38/MK2 pathway in response to stress stimuli.  
589 *Biochem J* 2013;**452**:531-43.
- 590 (45) Thompson MP, Kim D. Links between fatty acids and expression of UCP2 and UCP3  
591 mRNAs. *FEBS Lett* 2004;**568**:4-9.
- 592 (46) Carracedo A, Cantley LC, Pandolfi PP. Cancer metabolism: fatty acid oxidation in the  
593 limelight. *Nat Rev Cancer* 2013;**13**:227-32.
- 594 (47) Liu X, Zheng H, Yu WM, Cooper TM, Bunting KD, Qu CK. Maintenance of mouse  
595 hematopoietic stem cells ex vivo by reprogramming cellular metabolism. *Blood*  
596 2015;**125**:1562-5.
- 597 (48) Ito K, Carracedo A, Weiss D, Arai F, Ala U, Avigan DE, et al. A PML-PPAR-delta  
598 pathway for fatty acid oxidation regulates hematopoietic stem cell maintenance. *Nat Med*  
599 2012;**18**:1350-8.
- 600 (49) Lu L, Chen Y, Zhu Y. The molecular basis of targeting PFKFB3 as a therapeutic strategy  
601 against cancer. *Oncotarget* 2017;**8**:62793-802.
- 602 (50) Zhu W, Ye L, Zhang J, Yu P, Wang H, Ye Z, et al. PFK15, a Small Molecule Inhibitor of  
603 PFKFB3, Induces Cell Cycle Arrest, Apoptosis and Inhibits Invasion in Gastric Cancer.  
604 *PLoS One* 2016;**11**:e0163768.
- 605 (51) O'Neal J, Clem A, Reynolds L, Dougherty S, Imbert-Fernandez Y, Telang S, et al.  
606 Inhibition of 6-phosphofructo-2-kinase (PFKFB3) suppresses glucose metabolism and the  
607 growth of HER2+ breast cancer. *Breast Cancer Res Treat* 2016;**160**:29-40.
- 608 (52) Reddy MM, Fernandes MS, Deshpande A, Weisberg E, Inguilizian HV, Abdel-Wahab O,  
609 et al. The JAK2V617F oncogene requires expression of inducible  
610 phosphofructokinase/fructose-bisphosphatase 3 for cell growth and increased metabolic  
611 activity. *Leukemia* 2012;**26**:481-9.

612

613 **Figure Legends**

614 **Figure 1. NOX-derived ROS promotes transcriptional change in N-RAS<sup>G12D</sup> expressing**  
615 **HSPC and AML patient blasts and identifies the glycolytic pathway as a major target of**  
616 **ROS. (A)** Summary flow diagram showing the strategy for changes in mRNA expression  
617 analysed by Affymetrix microarray. Four treatment conditions were employed for the  
618 examination of the effect of N-RAS<sup>G12D</sup> and ROS on mRNA gene expression: CD34<sup>+</sup> HSPC  
619 infected with control vector ('C') or N-RAS<sup>G12D</sup> ('N'), incubated in the presence or absence of  
620 100nM DPI for 24 h to determine the ROS-specific gene expression profile (n=4). We examined  
621 changes that were only co-directional (i.e. they were similarly dysregulated in each replicate).  
622 **(B)** Significantly changing GeneGo<sup>TM</sup> Maps in human HSPCs as a response to changes in  
623 exposure to ROS. **(C)** Statistically significant changes in mRNA showing the impact of DPI  
624 (unfilled bars) on N-RAS<sup>G12D</sup> dependent target gene expression (filled bars). Non-specific  
625 effects of DPI were excluded as described in (A). Only genes involved in carbohydrate  
626 metabolism using the Human Exon 1.0<sup>ST</sup> Full Probe Set list were analysed. Statistically  
627 significant gene changes in Control cells treated with DPI compared to untreated control were  
628 excluded from the final list. Data represents mean fold change of n=4; P value calculated by 2-  
629 way ANOVA with Bonferroni multiple testing correction. **(D)** Hierarchical clustering of patient  
630 AML mRNA expression z-Scores based on RNA Seq V2 RSEM. NOX2 high / low expressing  
631 blasts was defined as, above and below the median expression intensity of NOX2 (aka *CYBB*).  
632 Genes involved in glycolysis and carbohydrate transport are shown (as defined by Affymetrix  
633 Netaffx<sup>TM</sup> gene annotation software under advanced pathway searches); AML patient blasts

634 (n=160). Boxed section shows cluster of genes associated with NOX2 high AML blasts. **(E)**  
635 Expression of genes from AML patient blasts significantly correlating with NOX2 (*CYBB*,  
636  $R > 0.5$ ) expression. R; Spearman's Correlation coefficient. FDR, False Discovery Rate; GLUT3  
637 (SLC2A3), glucose transporter 3; GLUT5 (SLC2A5), glucose transporter 5; GLUT6 (SLC2A6),  
638 glucose transporter 6; GLUT14 (SLC2A14), glucose transporter 14; HK, hexokinase; PFKFB, 6-  
639 phosphofructo-2-kinase/fructose-2,6-bisphosphatase; PFK(P). phosphofructokinase platelet;  
640 FBP1, fructose-1,6-bisphosphatase 1; ENO, enolase; PK(M), pyruvate kinase muscle; LDH(A),  
641 lactate dehydrogenase A; MCT4 (SLC16A3), monocarboxylate transporter 4.

642 **Figure 2. ROS promotes glucose uptake.** **(A)** 'Medium' - following transduction, N-RAS<sup>G12D</sup>  
643 were cultured for 3 days without growth factors, glucose present in the media was assayed using  
644 a fluorometric glucose kit (n=4) (see methods) and normalised to empty-vector control. Glucose  
645 uptake in the cell is inversely proportional to the glucose remaining in the media. '2-NBDG' -  
646 glucose uptake using the fluorogenic substrate 2-NBDG (normalised to control) in N-RAS<sup>G12D</sup>  
647 HSPC (n=4) cultured as above. **(B)** Glucose uptake (normalised to Wild Type (WT) control) *ex*  
648 *vivo* in N-RAS<sup>G12D</sup> bone marrow compared to WT control cells (n=8). **(C)** N-RAS<sup>G12D</sup> HSPCs  
649 (day 5 post infection) were treated with 100nm DPI and cultured for 24 h without growth factors.  
650 Glucose in culture media (normalised to untreated control) was assayed (n=3). Glucose uptake  
651 in the cell is inversely proportional to the glucose remaining in the media. N-RAS<sup>G12D</sup> HSPCs  
652 were treated with 5µM VAS-2870 (VAS; n=3) or 300mU/mL PEGylated catalase (Cat; n=2) for  
653 24 h and glucose uptake assayed using 2-NBDG (normalised to PEG-treated control). **(D)**  
654 Concentration of extracellular L-lactate in culture media of transduced CD34<sup>+</sup> cells (cultured as

655 above) treated with 5  $\mu$ M VAS-2870 as above (n=4). Data represents mean $\pm$ 1SD. \* denotes  
656 p<0.05 and \*\* p<0.001 analysed by one sample t-test.

657 **Figure 3. Overproduction of ROS is associated with changes in glucose utilizations in**  
658 **primary AML blasts.** Data from global biochemical profiling of AML blasts stratified  
659 according to extracellular ROS production was performed. **(A)** Principal components analysis of  
660 global biochemical profiling of AML cells with high and low ROS production; ROS<sup>Low</sup>, n=10;  
661 ROS<sup>high</sup>, n=10. Also shown are normal human mononuclear control cells (Ctrl\_MN: n=4). **(B)**  
662 Summary of the numbers of biochemicals that achieved statistical significance (\*p $\leq$ 0.05), as well  
663 as those approaching significance (<sup>#</sup>0.05<p<0.10) analysed by Welch's two sample t-test.  
664 Levels of biochemicals normalised to total protein in **(C)** glycolysis and **(D)** Pentose Phosphate  
665 Pathway (PPP) are shown.

666 **Figure 4. PFKFB3 protein expression correlates with levels of NOX2 derived extracellular**  
667 **ROS.** **(A)** Human CD34<sup>+</sup> HSPC control and N-RAS<sup>G12D</sup> (day 5 post transduction) were cultured  
668 for 24 h in cytokine free media in the presence or absence of DPI (100nM) followed by whole  
669 cell protein extraction. (i) Example western blot of PFKFB3 protein expression. (ii) Relative  
670 protein expression (as measured by pixel densitometry of equivalent regions of interest (ROI)  
671 between different samples on the same blot then normalised to control) of PFKFB3 (n=3). **(B)**  
672 Western blot showing PFKFB3 protein expression levels in THP-1 cells with NOX2 knocked  
673 down (KD) or cells treated with DPI (100nM) for 24 h compared to control (non-mammalian  
674 shRNA) cells. Lower panel showing relative protein expression of PFKFB3 compared to control  
675 (n=3). **(C)** Percentage proliferative change (normalised to control) in THP-1 cells with NOX2  
676 KD (n>3) over 72 h. **(D)** Glucose uptake in single cell analysis using 2-NBDG (normalised to

677 control) in THP-1 cells with NOX2 KD (n=4) or THP-1 cells treated with 300 mU/mL  
678 PEGylated catalase (Cat; n=6). **(E)** Western blot showing PFKFB3 protein expression in  
679 Mv4;11 cells treated with glucose oxidase (GOX) (10 and 20mU/mL for 24 h), which catalyses  
680 production of hydrogen peroxide (H<sub>2</sub>O<sub>2</sub>) in cell culture media; (imitating the effect of NOX2-  
681 generated ROS production). Lower panel showing relative protein expression of PFKFB3  
682 compared to control (n=3). Correlation of PFKFB3 overexpression in Mv4;11 cells treated with  
683 GOX for 24 h on **(F)** proliferation and **(G)** glucose uptake using 2-NDBG (n=5). Actin was used  
684 as a loading control. Data represents mean±1SD. † denotes p<0.05 analysed by ANOVA with  
685 Tukey's honestly significance difference. \* denotes p<0.05 analysed by one sample t-test.

686 **Figure 5. Effect of PFKFB3 overexpression and knock down on proliferation and glucose**  
687 **uptake in leukemia cells.** **(A)** Western blot analysis of PFKFB3 protein comparing control and  
688 PFKFB3-overexpression (OE) Mv4;11 cells. Actin was used as a loading control. **(B)**  
689 Percentage proliferation (normalised to control) of Mv4;11 PFKFB3 over-expressed (OE) cells  
690 compared to control (n>3). **(C)** Glucose uptake in Mv4;11 PFKFB3-OE cells compared to  
691 control following 72 h (n=3). Glucose was assayed in the culture media and glucose uptake in  
692 the cell is inversely proportional to the glucose remaining in the media. The concentration of  
693 glucose in the culture media (starting concentration 25nmol/μL) of PFKFB3-OE cells after 24 h  
694 was 15nmol/μL compared with 23nmol/μL in control cells. **(D)** Western blot analysis of  
695 PFKFB3 protein comparing control (non-mammalian targeting shRNA control) and PFKFB3  
696 knock down (KD) in THP-1 cells. Actin was used as a loading control. **(E)** Percentage  
697 proliferation (normalised to control) of THP-1 PFKFB3-KD cells compared to control (n>3). **(F)**  
698 Glucose uptake in single cell analysis using 2-NDBG (normalised to control) of THP-1  
699 PFKFB3-KD cells compared to control following 24h growth (n=5). Data represents

700 mean±1SD. † denotes p<0.05 analysed by ANOVA with Tukey's honestly significance  
701 difference. \*\*\*p<0.005 denotes statistical significance calculated by Student's t-test calculated.

702 **Figure 6. ROS induced changes in PFKFB3 expression is mediated via UCP/p-AMPK. (A)**

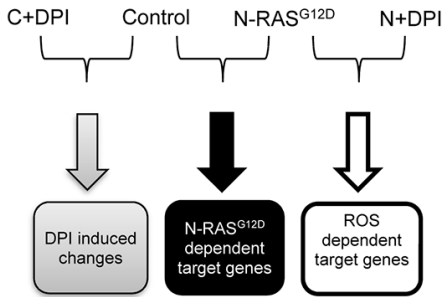
703 Normalised log<sub>2</sub> expression of *HIFA* (transcript ID 3567728) mRNA in control HSPC, DPI, N-  
704 RAS<sup>G12D</sup> HSPC and N-RAS<sup>G12D</sup> HSPC treated with DPI (100nM). Box plots represent median  
705 quartile ranges, x represents mean value (n=4). p-Value calculated by 2-way ANOVA with  
706 Bonferroni multiple testing correction. **(B)(i)** Western blot showing expression of HIF-1α in  
707 control THP-1, THP-1 NOX2-KD and THP-1 cells treated with DPI as (A). As positive  
708 controls, THP-1 cells were treated with CoCl<sub>2</sub> as indicated (an inhibitor of HIF-1α degradation  
709 (50)). HIF-1α recombinant protein were also immunoblotted. Actin was used as loading control.  
710 **(B)(ii)** Western blot showing expression of HIF-1α, comparing control THP-1 (non-mammalian  
711 shRNA target) and THP-1 HIF-1α knocked down (KD). Cells were also untreated or treated  
712 with CoCl<sub>2</sub> as above. **(C)** Western blot showing expression of PFKFB3 in THP-1 cells knocked  
713 down with HIF1-α. **(D)** Glucose uptake (normalised to control) of THP HIF-1α KD cells (n=3).  
714 Data represents mean±1SD. **(E)** Immunoblot showing PFKFB3, UCP2 and p-AMPK expression  
715 upon 1 h pre-treatment of Mv4;11 cells with the UCP2 inhibitor Genipin (5μM) followed by  
716 GOX treatment for 24 h. **(F)** Glucose uptake using 2-NBDG (normalised to untreated cells;  
717 control) of Mv4;11 cells treated with GOX (20mU/mL) and / or Genipin (5μM) (n=5). Data  
718 represents mean±1SD. \*\*\*p<0.005 and §p<0.01 denotes statistical significance calculated by  
719 Student's t-test calculated.

720 **Figure 7. Targeting PFKFB3 reduces glucose uptake and cell proliferation in AML cells.**

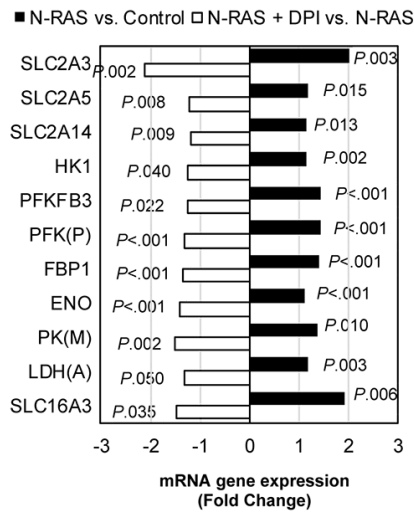
721 Glucose uptake using 2NBDG (normalised to untreated control) in THP-1 cells lines treated with

722 (A) 3PO or (B) PFK158 for 24 h. Vehicle control for 3PO and PFK158 was DMSO 0.05% and  
723 DMSO 0.01% respectively. Data represents mean±1SD (n>3). Proliferation (normalised to  
724 control) in THP-1 cells, seeded at  $4 \times 10^5$ /mL treated with (C) 3PO or (D) PFK158. Vehicle  
725 control for 3PO, DMSO 0.05% (n=6). Vehicle control for PFK158, DMSO 0.01% (n=6). (E)  
726 Glucose uptake using 2NBDG (normalised to untreated control) in Mv4;11 cells treated with  
727 inhibitors to PFKFB3 and/or incubated with 10 mU/mL GOX (source of H<sub>2</sub>O<sub>2</sub>) (n=3). (F)  
728 Representative flow cytometric bivariate plots from bone marrow harvested from tibias and  
729 femurs of adult NSG mice (7-10 weeks old) sub-lethally irradiated with 200cGy total body  
730 irradiation 24 h before injection of control THP-1 cells or THP-1 cells where PFKFB3 was KD.  
731 Human cells were distinguished from mouse cells using hCD45-FITC, hCD33-APC and  
732 mCD45-PerCP-Cy5.5 antibodies. Uninoculated NSG mice were used to control for the analysis  
733 of THP-1 engraftment (n=4) and analysed at week 6. Data represents mean±1SD. † denotes  
734 p<0.05 and represent significantly different groups from control, analysed by ANOVA with  
735 Tukey's honestly significance difference. \*\*\* p<0.005 denotes statistical significance calculated  
736 by Student's t-test calculated.

**A**



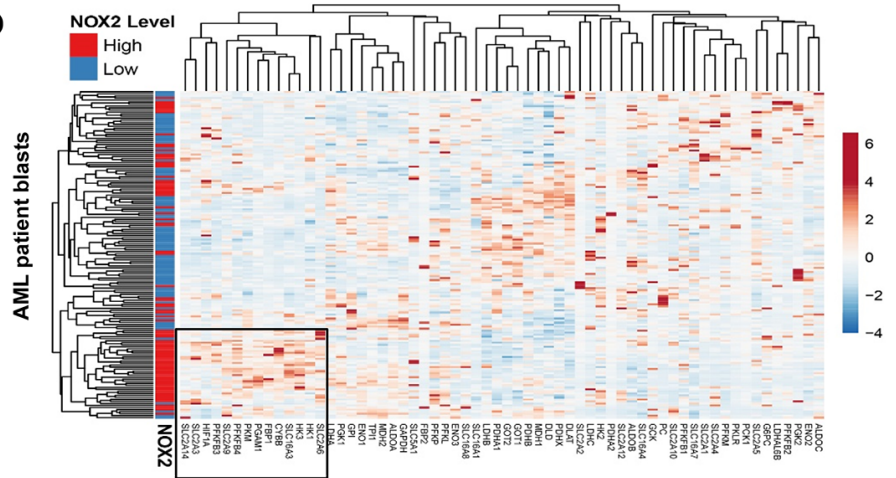
**C**



**B**

#	GeneGo™ Pathway Maps	p-value	FDR
1	Glycolysis and gluconeogenesis (short map)	1.982e-8	8.324e-7
2	Fructose metabolism	2.448e-6	5.141e-5
3	Fructose metabolism/ Rodent version	4.101e-6	5.741e-5
4	Glycolysis and gluconeogenesis p. 1	3.208e-5	3.368e-4
5	Development regulation of endothelial progenitor cell differentiation from adult stem cells	3.000e-3	2.520e-2
6	Urea cycle	4.197e-3	2.882e-2
7	(L)-Arginine metabolism	4.804e-3	2.882e-2
8	Arginine metabolism/ Rodent version	6.999e-3	3.675e-2
9	Glycine, serine, cysteine and threonine metabolism	1.212e-2	5.251e-2
10	Glycine, serine, cysteine and threonine metabolism/ Rodent version	1.250e-2	5.251e-2

**D**



**E**

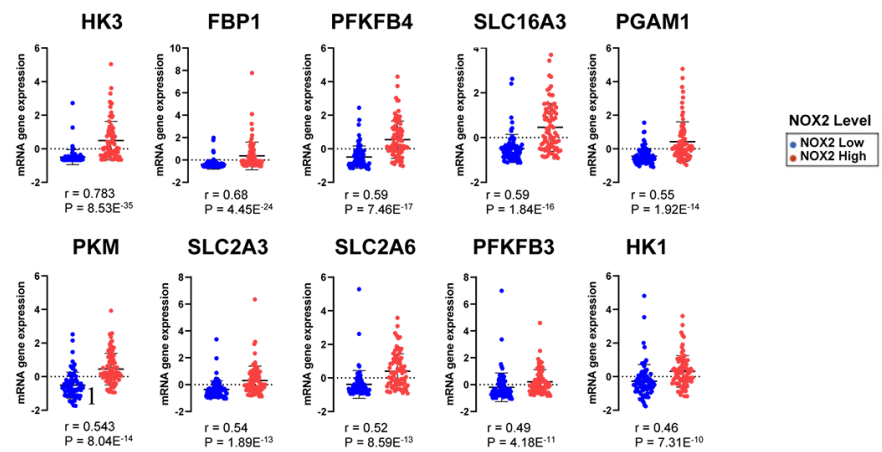


**Figure 1**

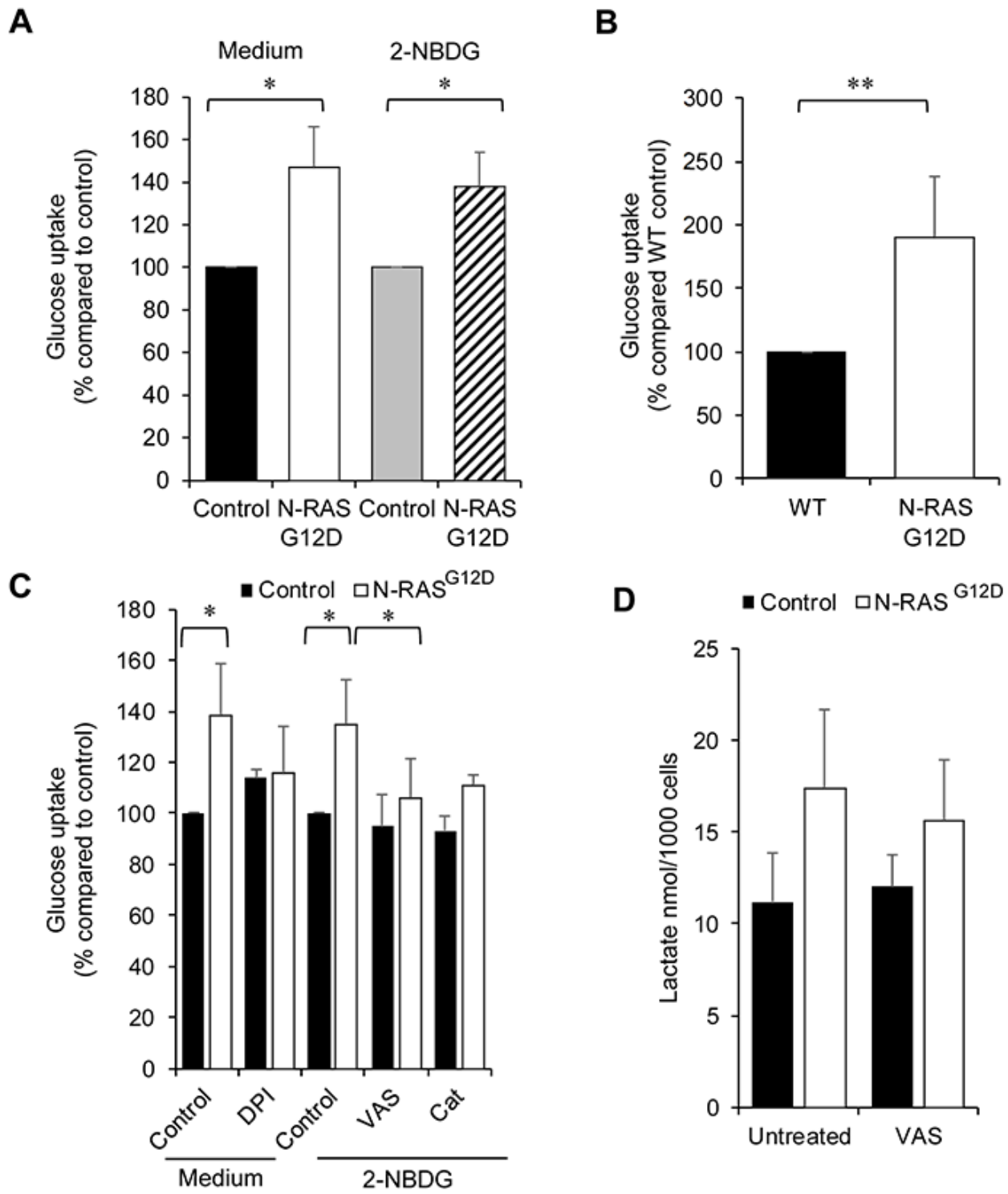
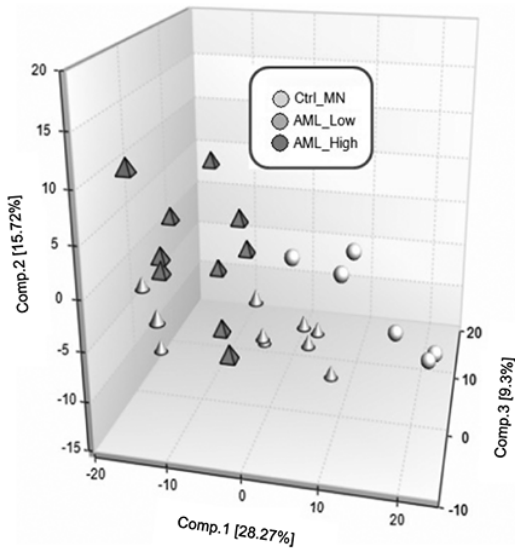
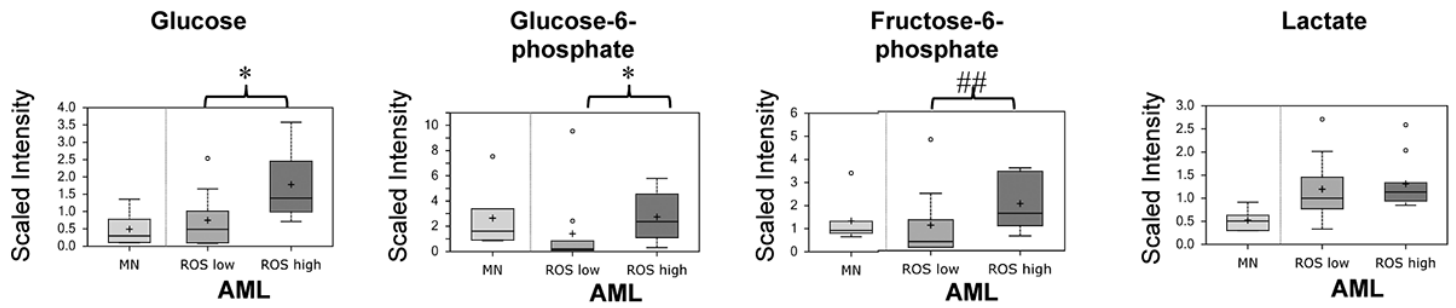
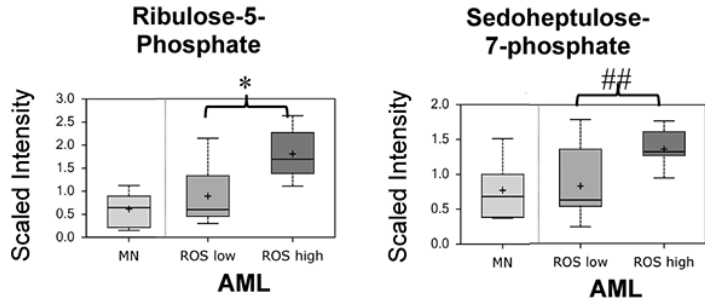


Figure 2.

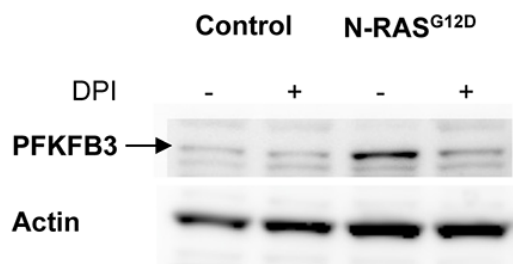
**A****B**

Significantly altered Biochemicals	Total Biochemicals P≤0.05	Biochemicals (↑/↓)	Total Biochemicals 0.05<p<0.10	Biochemicals (↑/↓)
<b>AML ROS<sup>Low</sup></b> Ctrl MN	208	172/36	101	76/25
<b>AML ROS<sup>High</sup></b> Ctrl MN	268	240/28	94	76/18
<b>AML ROS<sup>High</sup></b> <b>AML ROS<sup>Low</sup></b>	97	76/21	99	66/33

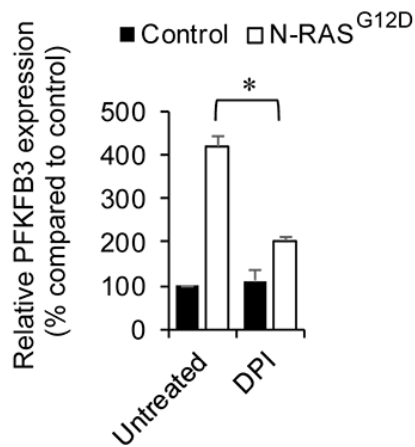
**C****D****Figure 3.**

## A CD34<sup>+</sup> primary cells

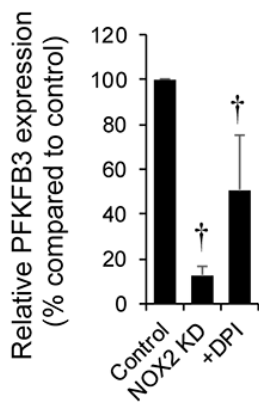
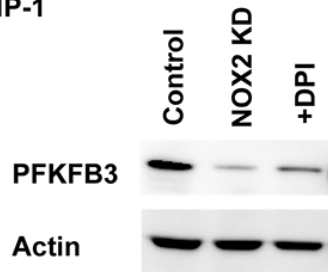
(i)



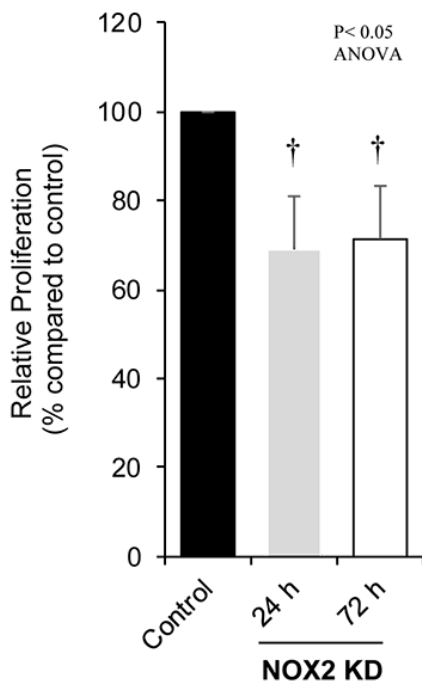
(ii)



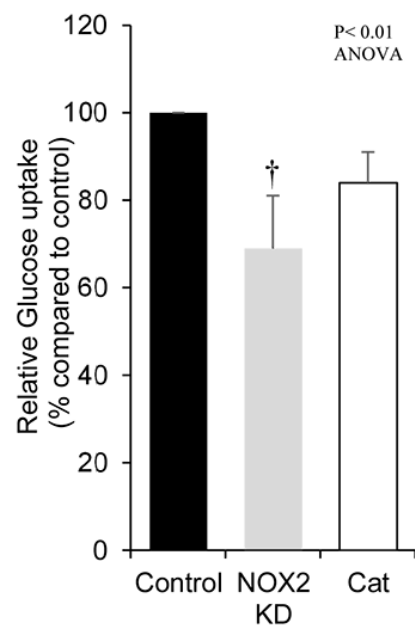
## B THP-1



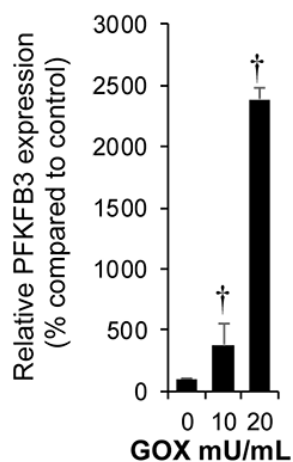
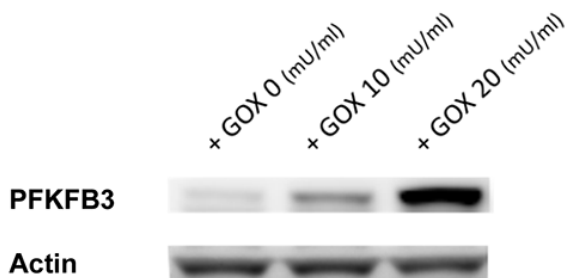
## C THP-1



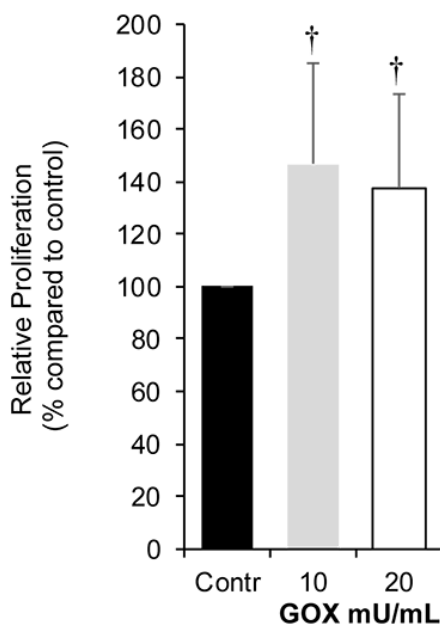
## D THP-1



## E Mv4;11



## F Mv4;11



## G Mv4;11

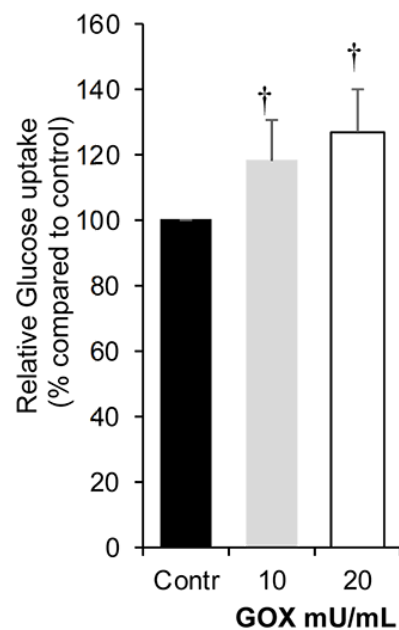
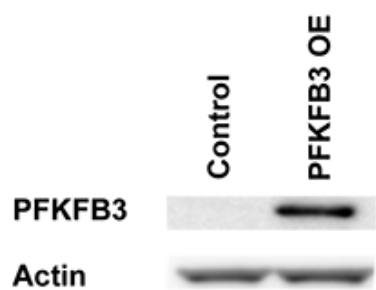
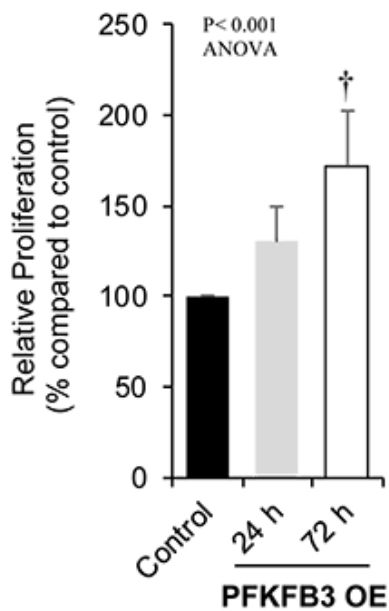


Figure 4

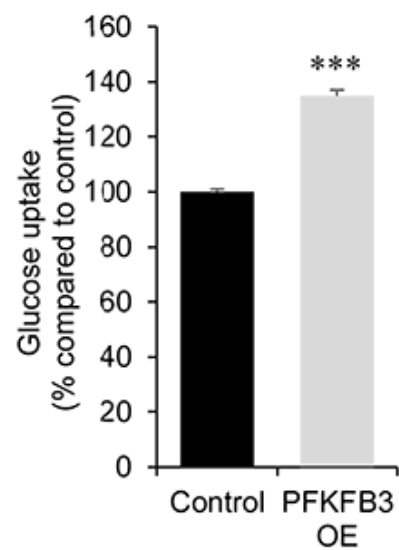
**A** Mv4;11



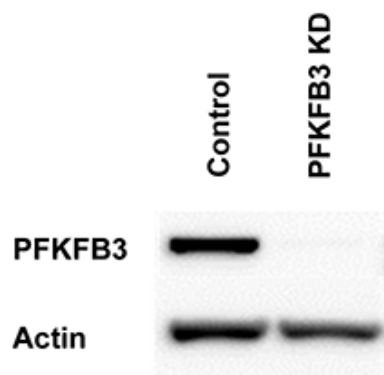
**B** Mv4;11



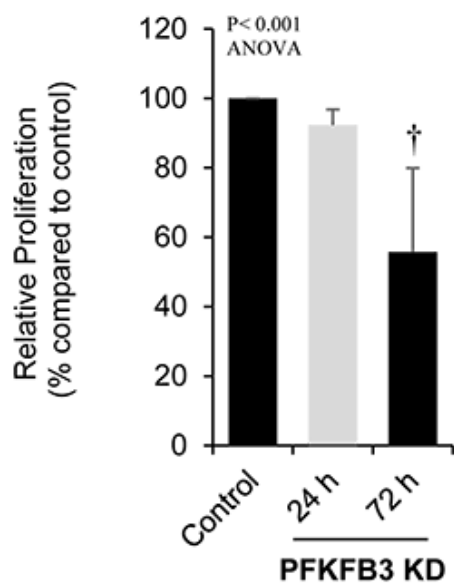
**C** Mv4;11



**D** THP-1



**E** THP-1



**F** THP-1

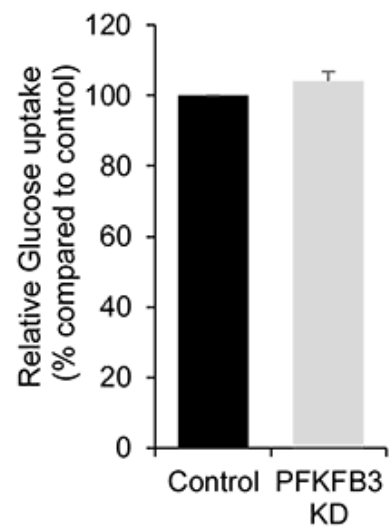
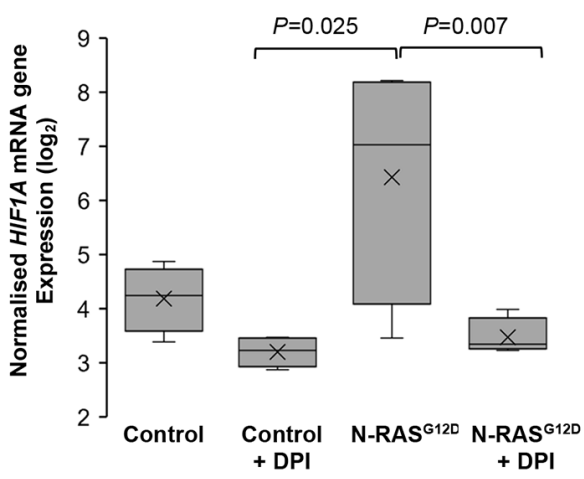
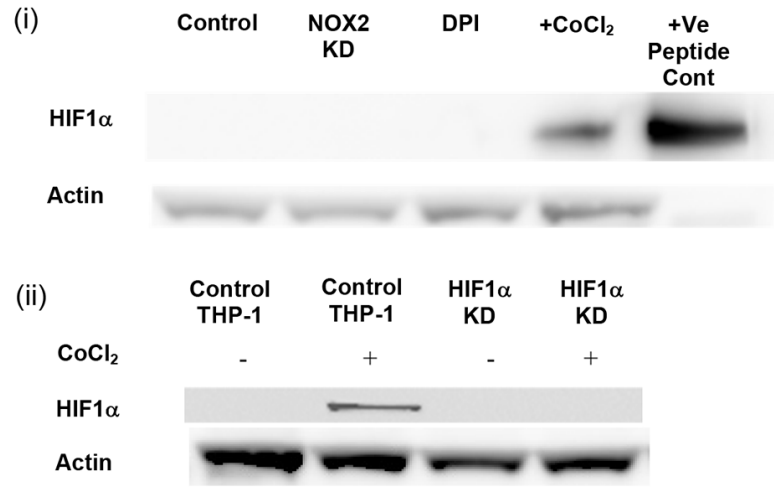


**Figure 5.**

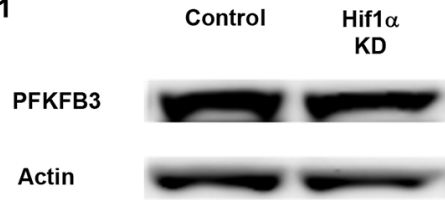
### A CD34<sup>+</sup> primary cells



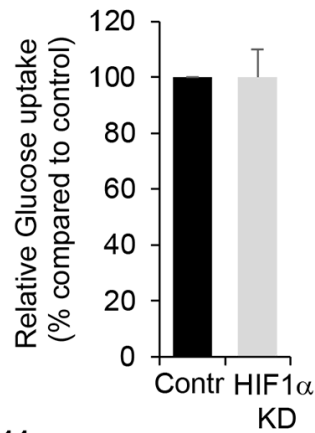
### B THP-1



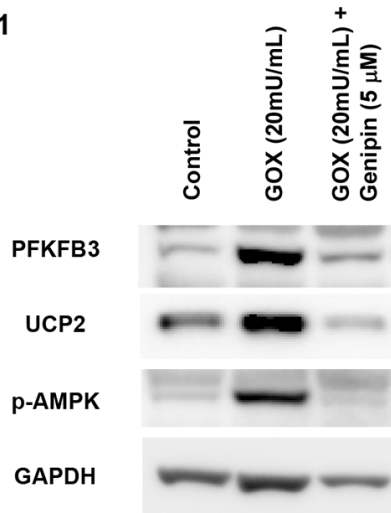
### C THP-1



### D



### E Mv4;11



### F Mv4;11

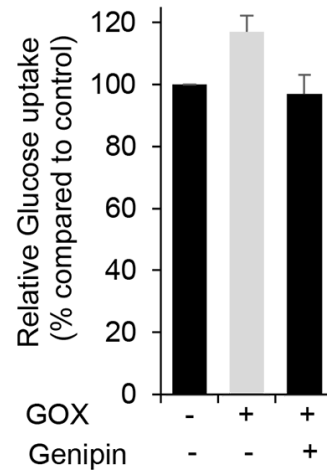
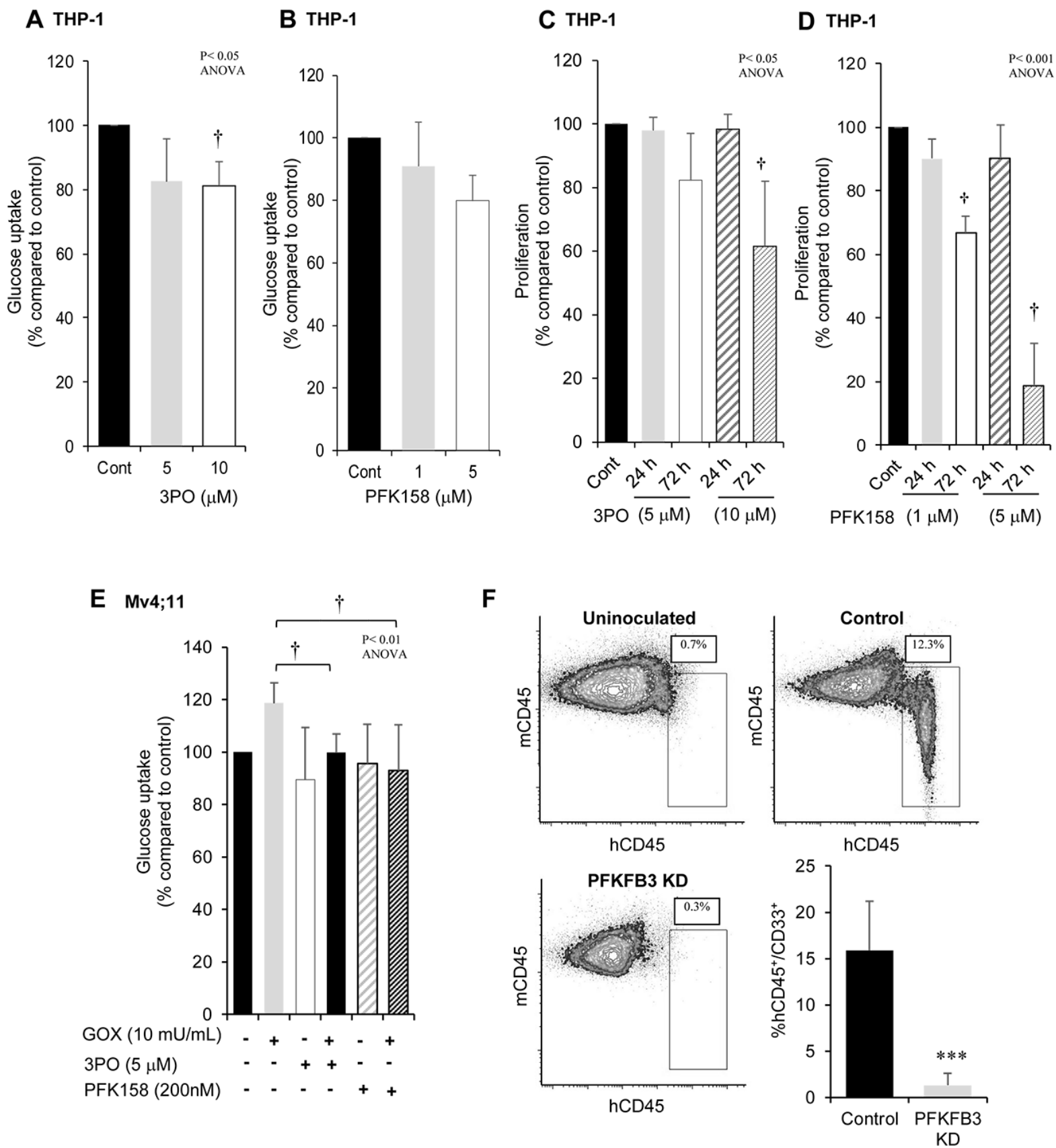


Figure 6.



**Figure 7**